Enhanced performance of polymer:fullerene bulk heterojunction solar cells upon graphene addition

Pieter Robaeys,[1,a)] Francesco Bonaccorso,[2,3] Emilie Bourgeois,[1,4] Jan D'Haen,[1,4] Wouter Dierckx,[1] Wim Dexters,[1] Donato Spoltore,[1] Jeroen Drijkoningen,[1] Jori Liesenborgs,[5] Antonio Lombardo,[2] Andrea C. Ferrari,[2] Frank Van Reeth,[5] Ken Haenen,[1,4] Jean V. Manca,[1,4] and Milos Nesladek[1,4]

[1]*Institute for Materials Research (IMO), Hasselt University, Belgium*
[2]*Cambridge Graphene Centre, University of Cambridge, 9 JJ Thomson Avenue, Cambridge, United Kingdom*
[3]*Istituto Italiano di Tecnologia, Graphene Labs, Via Morego 30, 16163 Genova, Italy*
[4]*IMOMEC, IMEC vzw, Belgium*
[5]*Expertise centre for Digital Media (EDM), Hasselt University, Belgium*

(Received 1 April 2014; accepted 3 July 2014; published online 28 August 2014)

Graphene has potential for applications in solar cells. We show that the short circuit current density of P3HT (Poly(3-hexylthiophene-2,5-diyl):PCBM((6,6)-Phenyl C61 butyric acid methyl ester) solar cells is enhanced by 10% upon the addition of graphene, with a 15% increase in the photon to electric conversion efficiency. We discuss the performance enhancement by studying the crystallization of P3HT, as well as the electrical transport properties. We show that graphene improves the balance between electron and hole mobilities with respect to a standard P3HT:PCBM solar cell. © *2014 AIP Publishing LLC*. [http://dx.doi.org/10.1063/1.4893777]

Polymer bulk heterojunction (BHJ) solar cells[1–3] bring advantages of low processing cost and mechanical flexibility compared to conventional inorganic solar cells.[4] Photon to electric power conversion efficiencies (PCE) up to 12% were reported.[5] Graphene and reduced graphene oxide (RGO) are promising materials for solar cells applications.[6] They have been used as transparent conductive electrodes (TCEs) in organic photovoltaic (OPV) cells to replace indium (ITO) and fluorine-doped tin oxide (FTO).[6–10] It was shown that GO can replace PEDOT:PSS (Poly(3,4-ethylenedioxythiophene)-poly(styrenesulfonate)) as an electron blocking layer in OPVs.[11] It was suggested that OPV cells containing graphene nanoribbons in the active layer can reach PCE ∼ 12%, due to charge carrier mobility (μ) enhancement.[12] In graphene-polymer composites, the electronic states of graphene overlap with those of the polymer molecules, leading to charge transfer (CT).[13] This enhances the CT rate, preventing recombination at the photoanode, thus improving PCE.[13–15]

In order to further increase the PCE, work has been done to chemically functionalize RGO with various polymeric or donor-acceptor systems, such as poly-3-hexyl thiophene-2,5-diyl (P3HT)[16] and [6,6]-Phenyl-C61-butyric acid methyl ester (PCBM).[17] Using quantum dots in solar cells based on small molecules DR3TBDT:[6,6]-phenyl-C71-butyric acid methyl ester (DR3TBDT:PC71M) led to a PCE ∼ 6.81.[18] Ternary blends, e.g., comprising either two polythiophene donors and a fullerene acceptor,[19] or a polythiophene donor and two fullerene acceptors,[19,20] were suggested to increase the short circuit current density (I_{SC}) of BHJ solar cells by increasing the light absorption window[19] or balancing the mobilities,[19] or by changing open circuit voltage (V_{OC}) by influencing the oxidation potential.[19–21] However, little is known about the effect of graphene on charge transport and CT when added as a ternary mixture to BHJ solar cells, while it is know that the organization of P3HT is a crucial factor determining the ultimate PCE.[22]

Here, we investigate the effect of the incorporation of sub-percolation amounts of graphene flakes in P3HT-PCBM solar cells on the PCE, the CT between P3HT and the PCBM acceptor, and the charge collection. We use the BHJ P3HT:PCBM solar cell as a model system because, even if such cells do not yield the highest PCE amongst BHJ solar cells, they are widely used,[1] cost-effective,[1] and easy to fabricate.[1] An important issue in P3HT:PCBM solar cells is the inadequate transport of photo-generated charge carriers,[1] which limits the charge collection at the photoanode.[1] In particular, hole transport is one of the main factors limiting the generated photo-current;[1] this is due to the fact that the hole mobility (μ_h) of the electron donating polymer is much lower than the electron mobility (μ_e) of commonly used acceptors.[1–3] Due to this mobility imbalance, a positive space charge builds up at the photoanode, leading to trapping of electrons near the back electrode.[23,24] Graphene, due to its high electrical conductivity (σ),[25] can act as a bridge structure in BHJs to help avoid charging. We show that the short circuit current density is enhanced by 10% by the addition of graphene, with a 15% increase in PCE. We find that graphene improves the balance between μ_e and μ_h with respect to a standard P3HT:PCBM solar cell.

Our cells are assembled following 3 steps: 1) preparation of the of graphene dispersion; 2) preparation of polymer dispersions and mixing with the graphene dispersion of step 1; 3) preparation of solar cells from the dispersions of step 2.

Step 1: 100 mg of Graphite flakes (Sigma Aldrich Ltd.) is dispersed in 10 ml of 1,2-dichlorobenzene (ODCB). The solvent is chosen for its compatibility with P3HT:PCBM.[26] Moreover, 1.2-dichlorobenzene has a surface tension of 37 mN/m,[27] which is close to that of ideal solvents for the dispersion of graphene flakes, such as N-Methyl2Pyrrolidone,[28]

a)pieter.robaeys@uhasselt.be

that minimize the interfacial tension between the liquid and the graphene flakes.[29] The dispersion is ultrasonicated for 10 hours and ultracentrifuged, exploiting sedimentation-based separation.[29–32] After ultracentrifugation, the supernatant is extracted by pipetting. Optical absorption spectroscopy (OAS) is used to evaluate the concentration, c, of graphitic material in dispersion, Fig. 1(a). Using the experimentally derived absorption coefficient of 1390 l/g at 660 nm,[29–31] we estimate $c \sim 0.02$ mg/ml. The graphene flakes in this dispersion are studied by Raman spectroscopy at 488, 514.5, and 633 nm. Fig. 1(b) shows a typical Raman spectrum. Besides the G and 2D peaks, it has significant D and D′ intensities and the combination mode D + D′. The G peak corresponds to the E_{2g} phonon at the Brillouin zone centre.[32–35] The D peak is due to the breathing modes of sp^2 rings and requires a defect for its activation by double resonance (DR).[32–34] The 2D peak is the second order of the D peak. This is a single peak in single layer graphene (SLG), whereas it splits into 4 peaks in bi-layer graphene, reflecting the evolution of the band structure. The 2D peak is always seen, even when no D peak is present, since no defects are required for the activation of two phonons with the same momentum, one backscattered from the other.[33] DR can also happen as intra-valley process, i.e., connecting two points belonging to the same cone around **K** or **K**′;[32,34] this process gives rise to the D′ peak. The 2D′ is the second order of the D′. Statistical analysis of the spectra shows that Pos(2D) peaks at $\sim 2702\ cm^{-1}$, Fig. 1(c), while FWHM(2D) varies from 50 to $95\ cm^{-1}$, Fig. 1(d). Pos(2G), Fig. 1(e), and FWHM(G), Fig. 1(f), are ~ 1582 and $\sim 27\ cm^{-1}$. The Raman spectra show significant D and D′ intensity, with an average intensity ratio $I(D)/I(G) \sim 0.90$, Fig. 1(g). This is attributed to the edges of our sub-micrometer flakes,[36] rather than to the presence of a large amount of structural defects within the flakes. This observation is supported by the low dispersion of the G peak, $Disp(G) < 0.04\ cm^{-1}$/nm, much lower than what expected for disordered carbon.[37] Combining I(D)/I(G) with FWHM(G) and Disp(G) allows us to discriminate between disorder localized at the edges and disorder in the bulk. In the latter case, a higher I(D)/I(G) would correspond to higher FWHM(G) and Disp(G). Figs. 1(i) and 1(l) show that Disp(G), I(D)/I(G), and FWHM(G) are not correlated, an indication that the major contribution to the D peak comes from the sample edges. The distribution of FWHM(2D) in Fig. 1(d) has two maxima ~ 57 and $\sim 77\ cm^{-1}$, the latter being the highest. This is consistent with the samples being a combination of SLG and few-layer graphene (FLG) flakes.

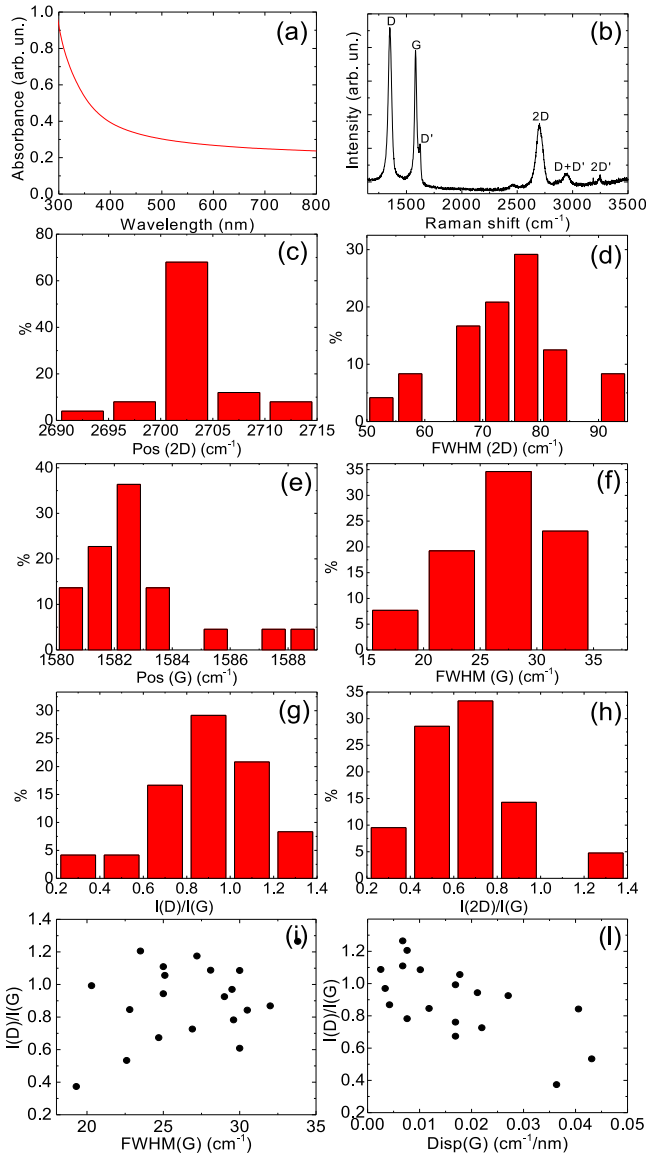

FIG. 1. (a) Optical absorption spectrum of graphene dispersion. (b) Raman spectrum measured at 514.5 nm excitation for a representative flake obtained via LPE of graphite. Distribution of (c) Pos(2D), (d) FWHM(2D), (e) Pos(G), (f) FWHM(G), (g) I(D)/I(G), (h) I(2D)/I(G). (i) Distribution of I(D)/I(G) as a function of FWHM(G), and (l) Disp(G).

Step 2: The P3HT:PCBM dispersion in ODCB is prepared with 10 mg/ml P3HT (Rieke) and 8 mg/ml PCBM (Solenne B.V.). The P3HT:PCBM-graphene dispersion is prepared by using the identical P3HT:PCBM dispersion in the ODCB-graphene supernatant, obtained by centrifugation, and stirred under nitrogen atmosphere for 24 h at 50 °C.

Step 3: PEDOT:PSS is deposited by spin-coating at 3000 rpm for 40 s on cleaned glass substrates with a 100 nm ITO coating. The layers are annealed for 20 minutes at 120 °C. After cooling, a 100 nm layer of P3HT:PCBM:graphene is deposited on the PEDOT-PSS by spin-coating in N_2. A counter electrode of 20 nm Calcium and 60 nm Aluminum is deposited by evaporation. The thickness of the devices, determined by profilometry, is 106 ± 10 nm for the P3HT:PCBM reference and 110 ± 12 nm for the P3HT:PCBM:graphene devices.

I-V characteristics are measured under air mass (AM) 1.5 using the solar simulator Newport Oriel-A (100 mW/cm^2). 100 nm thick P3HT:PCBM:graphene field effect transistors (FET) are prepared to determine μ, as for Ref. 38. The FETs (channel 10 mm wide and 30μm long) are assembled on a heavily n-doped Si substrate with a 200 nm SiO_2 layer as the gate dielectric, resulting in a gate capacitance of 16.9nF/cm^2. The Au nominal work function (−5.1 eV (Ref. 39)) and energy position of the P3HT highest occupied molecular orbital (HOMO) (−5.1 eV (Ref. 40)) have the same value, thus the energy barrier for the hole injection at the zero applied field is minimal.

The PCE of the solar cells prepared from an active blend containing 2 wt% graphene is measured on 4 different devices. The I-V characteristics (Fig. 2) show an enhancement of

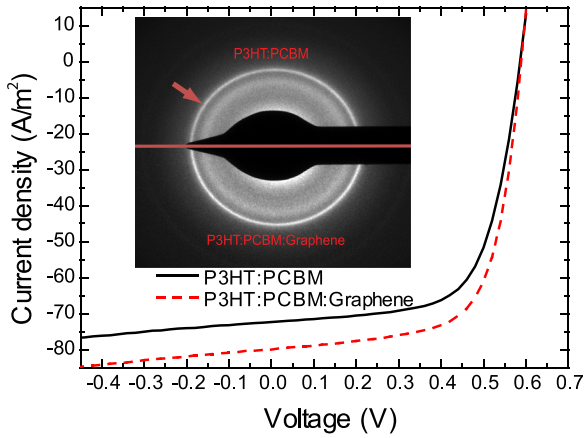

FIG. 2. Current voltage characteristics of P3HT:PCBM and P3HT:PCBM:graphene solar cells. The active layers are P3HT:PCBM (0.56:0.44), P3HT:PCBM:graphene (0.55:0.43:0.02). The inset shows the SAED images for P3HT:PCBM and P3HT:PCBM:graphene.

I_{sc} by a factor $\sim$10 A/m^2 compared to the P3HT:PCBM reference. The device fill factor (FF) is not influenced by the addition of graphene. V_{oc} also does not change significantly upon graphene addition. Atomic force microscopy (AFM) studies reveal that the surface topography of the active layer remains intact upon graphene addition. The P3HT:PCBM:graphene devices systematically show an increased PCE, from 2.79% for the reference device to 3.17% (see Table I).

To elucidate the influence of graphene on the P3HT crystallinity we use electron diffraction. Bright field transmission electron microscopy images are taken, combined with selected area electron diffraction (SAED), using a FEI Tecnai spirit at 120 kV. The diffraction rings in the inset of Fig. 2, marked by the red arrows, correspond to the diffraction patterns of P3HT. In the P3HT:PCBM:graphene samples, this ring becomes thinner and brighter, indicating a higher crystallization of P3HT.[41] This could originate from the structural organization of P3HT molecules upon graphene addition.[41] The crystallization of P3HT around molecules such as perylene tetracarboxydiimide was also reported in Ref. 42. We anticipate that the higher crystallinity of P3HT might improve μ. In addition, when μ_e and μ_h are unbalanced (i.e., have different values), the charge carrier with lower μ (usually the hole) limits transport[23,24] and results in charge accumulation at the contact/polymer interface. To study μ_e and μ_h upon graphene addition, we prepared FET structures with P3HT:PCBM and P3HT:PCBM:graphene, respectively.

TABLE I. Summary of solar cell parameters for our devices.

Configuration	Weight fractions	V_{OC} (V)	I_{SC} (A/m^2)	FF	η
P3HT:PCBM	0.56:0.44	0.6	72.55	0.65	2.79
P3HT:PCBM:Graphene	0.55:0.43:0.02	0.6	79.11	0.66	3.17

Fig. 3(a) shows that for the reference P3HT:PCBM, $\mu_e \sim 2\mu_h$. The 2 wt. % addition of graphene enhances μ_h by $\sim$30% and, at the same time, reduces μ_e by $\sim$50%. In BHJ solar cells, photo-generated holes are transported in the P3HT layer while photo-generated electrons are transferred to PCBM, from where they are transported through the PCBM by percolation.[43] While the μ_h increase could be linked to the P3HT crystallinity, we attribute the decrease in μ_e to charge trapping at the P3HT:PCBM-graphene interface.[44] When electrons are trapped, their mean drift velocity decreases.[44] However, the lowest ambipolar μ in the layer with 2 wt. % graphene is still higher than the lowest ambipolar μ in the reference layer, explaining why the reduced μ_e does not deteriorate solar cell performance. Due to the overlapping of the P3HT electron states with the π-electrons in graphene,[13] electrons can be directly transferred to a graphene flake.[15] The amount and type of the charge transported via graphene bridges will depend primarily on the characteristics of the graphene/P3HT interface and graphene doping. It was reported[45] that the use of N-doped graphene as a ternary component enhanced the PCE of P3HT:PCBM devices from 3% to 4.5% as consequence of enhanced electrical transport.[45] However, our data show that using graphene as the ternary component in BHJ balances μ_e and μ_h.

To support the experimental findings, we carry out simulations based on a two dimensional grid for the charge generation and recombination as for Ref. 46. We consider direct recombination, with the assumption that the charge carrier generation is field independent. The basic bi-molecular recombination, as described by the Langevin expression,[47,48] is used to describe the recombination kinetics. To show the effect of (in)balanced μ on the I/V characteristics of P3HT:PCBM solar cells, μ_h is varied between 5×10^{-5} and 1×10^{-3} cm^2/V s, while keeping the μ_e constant at 5×10^{-4} cm^2/V s (Fig. 3(b)). The most noticeable feature is the increase of I_{sc} and I_{max} (Fig. 3(b)), while μ_h is below μ_e. When $\mu_h = \mu_e$, I_{sc} is stable even when μ_h becomes larger than μ_e. The effect of the μ imbalance on both V_{oc} and V_{max} is less pronounced (Fig. 3(b)) with respect to I_{sc} and I_{max}. These simulations are in good agreement with experiments.

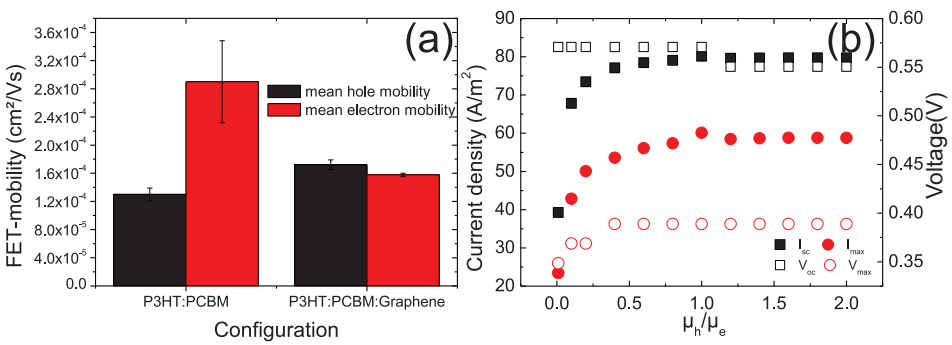

FIG. 3. (a) Field effect mobilities for 2 different conditions listed in Table I. (b) Effect of the solar cell parameters on changing hole mobility compared to the electron mobility. The simulation parameters are temperature 300 K, work function Ca/Al 3.41 eV, PEDOT 5.17 eV, LUMO acceptor level 4.1 eV, HOMO donor level 5.15 eV, generation rate 0.55×10^{28} cm^{-3}s^{-1}, relative permittivity 3.6, thickness 110 nm.

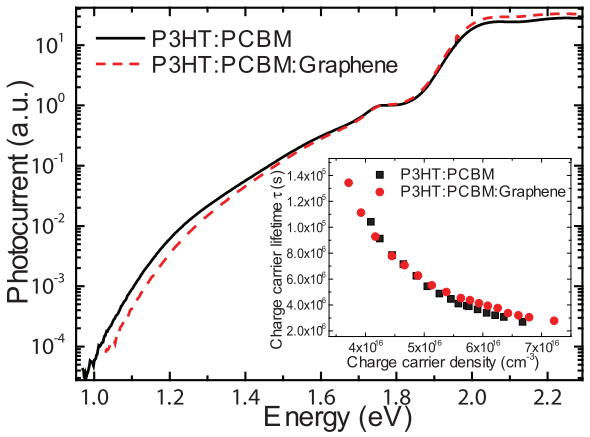

FIG. 4. Photocurrent spectra measured by FTPS. The inset plots the carrier lifetime as a function of the number of charges extracted from TPV data.

Fourier-transform photocurrent spectroscopy (FTPS) can be used as a probe for the charge transfer occurring in P3HT:PCBM solar cells.[49] We perform FTPS measurements using the modulated beam of a Thermo Electron Nicolet 8700 FTIR with an external detector, as for Ref. 50. The photocurrent generation in PCBM (band to band transition) is 1.75 eV, while the onset for the free photocarrier generation in P3HT is 1.9 eV.[49] The wide feature in the gap states (Fig. 4), CT band, is ascribed to the transitions between the lowest unoccupied molecular orbital (LUMO) of the acceptor and the highest occupied molecular orbital (HOMO) of the donor.[49] The FTPS spectra show a blue shift of the CT band of ~0.1 eV and the reduction of the gap states, after addition of 2 wt% graphene. The gap state reduction might be a reason for the observed change of the electron and hole trapping/recombination kinetics and μ_h/μ_e. We speculate that this effect may be a consequence of the structural changes of P3HT crystallinity.

To investigate the charge recombination effects,[51] transient photovoltage measurements (TPV) are performed, probing the recombination currents. The devices are kept at open circuit while illuminated with white light, used to control V_{oc}. A nitrogen pumped dye laser ($\lambda = 500$ nm) is used as optical perturbation, resulting in a voltage transient with an amplitude $\Delta V \sim V_{oc}$. Fig. 4 (inset) shows the recombination lifetime as a function of the charge carrier density. Although a CT blue-shift is seen in the FTPS-spectra (Fig. 4) while V_{oc} remains constant, there is no significant change in the ambipolar charge density or lifetime.[52] From these data, the recombination coefficient, i.e. the ratio between the number of charges and the recombination lifetime, does not change significantly. This explains the reduction of the recombination currents. Our data indicate that graphene, as the ternary component, does not decrease the charge carrier density and lifetime, thus keeping V_{oc} unchanged.

In conclusion, graphene addition to a P3HT:PCBM blend increases hole mobility, balances μ_h/μ_e, increases the photocurrent and enhances PCE in P3HT:PCBM BHJ solar cells.

We acknowledge funding from the UHasselt Special Research Fund (POLYDIAM), the Research Foundation-Flanders (G.05555.10N), a Royal Society Wolfson Research Merit Award, the European Research Council Grant Hetero2D, EU grants GENIUS, MEM4WIN, and Graphene Flagship (Contract No. 604391), EPSRC Grant Nos. EP/K01711X/1, EP/K017144/1, and EP/L016087/1, Nokia Research Centre, and a Newton International Fellowship.

[1]G. Dennler, M. C. Scharber, and C. J. Brabec, "Polymer-fullerene bulk-heterojunction solar cells," Adv. Mater. **21**(13), 1323–1338 (2009).
[2]C. Deibel, V. Dyakonov, and C. J. Brabec, "Organic bulk-heterojunction solar cells," IEEE J. Sel. Top. Quantum Electron. **16**(6), 1517–1527 (2010).
[3]C. Deibel, T. Strobel, and V. Dyakonov, "Role of the charge transfer state in organic donor-acceptor solar cells," Adv. Mater. **22**(37), 4097–4111 (2010).
[4]A. C. Mayer, S. R. Scully, B. E. Hardin, M. W. Rowell, and M. D. McGehee, "Polymer-based solar cells," Mater. Today **10**(11), 28–33 (2007).
[5]See http://www.heliatek.com/newscenter/latest_news/neuer-weltrekord-fur-organische-solarzellen-heliatek-behauptet-sich-mit-12-zelleffizienz-als-technologiefuhrer/?lang=en.
[6]F. Bonaccorso, Z. Sun, T. Hasan, and A. C. Ferrari, "Graphene photonics and optoelectronics," Nat. Photonics **4**(9), 611–622 (2010).
[7]I. Hamberg and C. G. Granqvist, "Evaporated Sn-doped {In2O3} films: Basic optical properties and applications to energy-efficient windows," J. Appl. Phys. **60**(11), R123–R160 (1986).
[8]A. E. Junge and W. O. Lytle, "Electroconductive products and production thereof," U.S. patent 2566346 A (1951).
[9]X. Wang, L. Zhi, and K. Müllen, "Transparent, conductive graphene electrodes for dye-sensitized solar cells," Nano Lett. **8**(1), 323–327 (2008).
[10]Y. Wang, X. Chen, Y. Zhong, F. Zhu, and K. P. Loh, "Large area, continuous, few-layered graphene as anodes in organic photovoltaic devices," Appl. Phys. Lett. **95**(6), 063302 (2009).
[11]S.-S. Li, K.-H. Tu, C.-C. Lin, C.-W. Chen, and M. Chhowalla, "Solution-processable graphene oxide as an efficient hole transport layer in polymer solar cells," ACS Nano **4**(6), 3169–3174 (2010).
[12]V. Yong and J. M. Tour, "Theoretical efficiency of nanostructured graphene-based photovoltaics," Small **6**(2), 313–318 (2010).
[13]Y. Wang, D. Kurunthu, G. W. Scott, and C. J. Bardeen, "Fluorescence quenching in conjugated polymers blended with reduced graphitic oxide," J. Phys. Chem. C **114**(9), 4153–4159 (2010).
[14]N. Yang, J. Zhai, D. Wang, Y. Chen, and L. Jiang, "Two-dimensional graphene bridges enhanced photoinduced charge transport in dye-sensitized solar cells," ACS Nano **4**(2), 887–894 (2010).
[15]A. Liscio, G. P. Veronese, E. Treossi, F. Suriano, F. Rossella, V. Bellani, R. Rizzoli, P. Samorì, and V. Palermo, "Charge transport in graphene–polythiophene blends as studied by Kelvin probe force microscopy and transistor characterization," J. Mater. Chem. **21**(9), 2924 (2011).
[16]B. K. Kuila, K. Park, and L. Dai, "Soluble P3HT-grafted carbon nanotubes: Synthesis and photovoltaic application," Macromolecules **43**(16), 6699–6705 (2010).
[17]D. Yu, K. Park, M. Durstock, and L. Dai, "Fullerene-grafted graphene for efficient bulk heterojunction polymer photovoltaic devices," J. Phys. Chem. Lett. **2**(10), 1113–1118 (2011).
[18]M. Li, W. Ni, B. Kan, X. Wan, L. Zhang, Q. Zhang, G. Long, Y. Zuo, and Y. Chen, "Graphene quantum dots as the hole transport layer material for high-performance organic solar cells," Phys. Chem. Chem. Phys. **15**(43), 18973–18978 (2013).
[19]T. Ameri, P. Khoram, J. Min, and C. J. Brabec, "Organic ternary solar cells: A review," Adv. Mater. **25**(31), 4245–4266 (2013).
[20]R. A. Street, D. Davies, P. P. Khlyabich, B. Burkhart, and B. C. Thompson, "Origin of the tunable open-circuit voltage in ternary blend bulk heterojunction organic solar cells," J. Am. Chem. Soc. **135**(3), 986–989 (2013).
[21]A. Gadisa, M. Svensson, M. R. Andersson, and O. Inganäs, "Correlation between oxidation potential and open-circuit voltage of composite solar cells based on blends of polythiophenes/ fullerene derivative," Appl. Phys. Lett. **84**(9), 1609–1611 (2004).
[22]G. Li, V. Shrotriya, J. Huang, Y. Yao, T. Moriarty, K. Emery, and Y. Yang, "High-efficiency solution processable polymer photovoltaic cells by self-organization of polymer blends," Nature Mater. **4**(11), 864–868 (2005).
[23]P. W. M. Blom, V. D. Mihailetchi, L. J. a. Koster, and D. E. Markov, "Device physics of polymer:fullerene bulk heterojunction solar cells," Adv. Mater. **19**(12), 1551–1566 (2007).

[24]M. Morana, P. Koers, C. Waldauf, M. Koppe, D. Muehlbacher, P. Denk, M. Scharber, D. Waller, and C. Brabec, "Organic field-effect devices as tool to characterize the bipolar transport in polymer-fullerene blends: The case of {P3HT-PCBM}," Adv. Funct. Mater. **17**(16), 3274–3283 (2007).
[25]A. K. Geim and K. S. Novoselov, "The rise of graphene," Nature Mater. **6**(3), 183–191 (2007).
[26]S. Günes, H. Neugebauer, and N. S. Sariciftci, "Conjugated polymer-based organic solar cells," Chem. Rev. **107**(4), 1324–1338 (2007).
[27]See http://www.microkat.gr/msdspd90-99/o-Dichlorobenzene.htm.
[28]Y. Hernandez, V. Nicolosi, M. Lotya, F. M. Blighe, Z. Sun, S. De, I. T. McGovern, B. Holland, M. Byrne, Y. K. Gun'Ko, J. J. Boland, P. Niraj, G. Duesberg, S. Krishnamurthy, R. Goodhue, J. Hutchison, V. Scardaci, A. C. Ferrari, and J. N. Coleman, "High-yield production of graphene by liquid-phase exfoliation of graphite," Nat. Nanotechnol. **3**(9), 563–568 (2008).
[29]F. Bonaccorso, A. Lombardo, T. Hasan, Z. Sun, L. Colombo, and A. C. Ferrari, "Production and processing of graphene and 2d crystals," Mater. Today **15**(12), 564–589 (2012).
[30]T. Hasan, F. Torrisi, Z. Sun, D. Popa, V. Nicolosi, G. Privitera, F. Bonaccorso, and A. C. Ferrari, "Solution-phase exfoliation of graphite for ultrafast photonics," Phys. Status Solidi **247**(11–12), 2953–2957 (2010).
[31]F. Torrisi, T. Hasan, W. Wu, Z. Sun, A. Lombardo, T. S. Kulmala, G.-W. Hsieh, S. Jung, F. Bonaccorso, P. J. Paul, D. Chu, and A. C. Ferrari, "Inkjet-printed graphene electronics," ACS Nano **6**(4), 2992–3006 (2012).
[32]O. M. Maragó, F. Bonaccorso, R. Saija, G. Privitera, P. G. Gucciardi, M. A. Iatì, G. Calogero, P. H. Jones, F. Borghese, P. Denti, V. Nicolosi, and A. C. Ferrari, "Brownian motion of graphene," ACS Nano **4**(12), 7515–7523 (2010).
[33]A. C. Ferrari and J. Robertson, "Origin of the 1150-cm-1 Raman mode in nanocrystalline diamond," Phys. Rev. B **63**(12), 121405 (2001).
[34]A. C. Ferrari, J. C. Meyer, V. Scardaci, C. Casiraghi, M. Lazzeri, F. Mauri, S. Piscanec, D. Jiang, K. S. Novoselov, S. Roth, and A. K. Geim, "Raman spectrum of graphene and graphene layers," Phys. Rev. Lett. **97**(18), 187401 (2006).
[35]F. Tuinstra and J. L. Koenig, "Raman spectrum of graphite," J. Chem. Phys. **53**(3), 1126–1130 (1970).
[36]C. Casiraghi, A. Hartschuh, E. Lidorikis, H. Qian, H. Harutyunyan, T. Gokus, K. S. Novoselov, and A. C. Ferrari, "Rayleigh imaging of graphene and graphene layers," Nano Lett. **7**(9), 2711–2717 (2007).
[37]A. C. Ferrari and J. Robertson, "Interpretation of Raman spectra of disordered and amorphous carbon," Phys. Rev. B **61**(20), 14095–14107 (2000).
[38]J.-C. Bolsée and J. Manca, "Effects of hole and electron trapping on organic field-effect transistor transfer characteristic," Synth. Met. **161**(9–10), 789–793 (2011).
[39]J. S. Kim, B. Lägel, E. Moons, N. Johansson, I. D. Baikie, W. R. Salaneck, R. H. Friend, and F. Cacialli, "Kelvin probe and ultraviolet photoemission measurements of indium tin oxide work function: A comparison," Synth. Met. **111–112**, 311–314 (2000).
[40]J. Y. Kim, K. Lee, N. E. Coates, D. Moses, T.-Q. Nguyen, M. Dante, and A. J. Heeger, "Efficient tandem polymer solar cells fabricated by all-solution processing," Science **317**(5835), 222–225 (2007).
[41]A. Chunder, J. Liu, and L. Zhai, "Reduced graphene oxide/poly(3-hexylthiophene) supramolecular composites," Macromol. Rapid Commun. **31**(4), 380–384 (2010).
[42]L. Bu, E. Pentzer, F. A. Bokel, T. Emrick, and R. C. Hayward, "Growth of {polythiophene/perylene} tetracarboxydiimide {donor/acceptor} Shish-Kebab nanostructures by coupled crystal modification," ACS Nano **6**(12), 10924–10929 (2012).
[43]C. Deibel and V. Dyakonov, "Polymer–fullerene bulk heterojunction solar cells," Rep. Prog. Phys. **73**(9), 096401 (2010).
[44]M. Lenes, S. W. Shelton, A. B. Sieval, D. F. Kronholm, J. C. (Kees) Hummelen, and P. W. M. Blom, "Electron trapping in higher adduct fullerene-based solar cells," Adv. Funct. Mater. **19**(18), 3002–3007 (2009).
[45]G. H. Jun, S. H. Jin, B. Lee, B. H. Kim, W.-S. Chae, S. H. Hong, and S. Jeon, "Enhanced conduction and charge-selectivity by N-doped graphene flakes in the active layer of bulk-heterojunction organic solar cells," Energy Environ. Sci. **6**(10), 3000–3006 (2013).
[46]K. Maturová, S. S. van Bavel, M. M. Wienk, R. A. J. Janssen, and M. Kemerink, "Description of the morphology dependent charge transport and performance of polymer:fullerene bulk heterojunction solar cells," Adv. Funct. Mater. **21**(2), 261–269 (2011).
[47]A. Pivrikas, G. Juska, T. Osterbacka, M. Westerling, M. Vilionas, K. Arlauskas, and H. Stubb, "Langevin recombination and space-charge-perturbed current transients in regiorandom poly(3-hexylthiophene)," Phys. Rev. B **71**(12), 125205 (2005).
[48]L. J. A. Koster, M. Kemerink, M. M. Wienk, K. Maturová, and R. A. J. Janssen, "Quantifying bimolecular recombination losses in organic bulk heterojunction solar cells," Adv. Mater. **23**(14), 1670–1674 (2011).
[49]K. Vandewal, K. Tvingstedt, A. Gadisa, O. Inganäs, and J. V. Manca, "On the origin of the open-circuit voltage of polymer–fullerene solar cells," Nature Mater. **8**(11), 904–909 (2009).
[50]K. Vandewal, L. Goris, I. Haeldermans, M. Nesládek, K. Haenen, P. Wagner, and J. V. Manca, "Fourier-transform photocurrent spectroscopy for a fast and highly sensitive spectral characterization of organic and hybrid solar cells," Thin Solid Films **516**(20), 7135–7138 (2008).
[51]A. Maurano, C. G. Shuttle, R. Hamilton, A. M. Ballantyne, J. Nelson, W. Zhang, M. Heeney, and J. R. Durrant, "Transient optoelectronic analysis of charge carrier losses in a selenophene/fullerene blend solar cell," J. Phys. Chem. C **115**(13), 5947–5957 (2011).
[52]K. R. Graham, P. Erwin, D. Nordlund, K. Vandewal, R. Li, G. O. Ngongang Ndjawa, E. T. Hoke, A. Salleo, M. E. Thompson, McGehee *et al.*, "Re-evaluating the role of sterics and electronic coupling in determining the open-circuit voltage of organic solar cells," Adv. Mater. **25**(42), 6076–6082 (2013).